Earth and Planetary Science Letters 584 (2022) 117456

Contents lists available at ScienceDirect

Earth and Planetary Science Letters

www.elsevier.com/locate/epsl

Geomorphic imprints of lithospheric flexure in central Australia

J.D. Jansen [a,*], M. Sandiford [b], T. Fujioka [c], T.J. Cohen [d], M. Struck [e], S.P. Anderson [f], R.S. Anderson [f], K. Wilcken [g], D.L. Egholm [h]

[a] GFÚ Institute of Geophysics, Czech Academy of Sciences, Prague, Czechia
[b] School of Earth Sciences, University of Melbourne, Melbourne, Australia
[c] Centro Nacional de Investigación sobre la Evolución Humana (CENIEH), Burgos, Spain
[d] School of Earth, Atmospheric & Life Sciences, University of Wollongong, Wollongong, Australia
[e] BAW Federal Waterways Engineering & Research Institute, Karlsruhe, Germany
[f] Department of Geological Sciences, University of Colorado, Boulder, CO, USA
[g] Australian Nuclear Science & Technology Organisation, Lucas Heights, Australia
[h] Department of Geoscience, Aarhus University, Aarhus, Denmark

ARTICLE INFO

Article history:
Received 14 February 2021
Received in revised form 30 January 2022
Accepted 21 February 2022
Available online xxxx
Editor: A. Webb

Keywords:
landscape evolution
bedrock fluvial incision
cosmogenic nuclides
gravity anomalies
mantle flow
central Australia
epigenetic gorge

ABSTRACT

The Finke River in central Australia is counted among the world's oldest drainage systems; this raises the prospect of investigating how (tectonic and sub-lithospheric) processes have shaped the landscape in the long term. The Finke's upper reaches display an enigmatic set of intertwined active and relict bedrock gorges that suggest a complex history of incision, aggradation and re-incision. We measured cosmogenic ^{10}Be and ^{26}Al in fluvial gravels preserved in the gorges, and we applied a Markov chain-Monte Carlo-based inversion model to test two limiting-case hypotheses about the timing of gravel deposition and exhumation. Our results suggest that the nuclide memory contained within the gravels was essentially erased during sediment storage exceeding several million years. Previous studies attribute central Australia's geomorphic development to intensified post-Miocene aridity in tune with the perception of a quiescent tectonic regime. However, the close correlation between drainage patterns and gravity anomalies leads us to propose, instead, that cyclical in-plane loading in the presence of extreme lithospheric density anomalies caused to-and-fro tilting of the upper Finke. We show that relief variations of order 100 m accompany mild in-plane loading of ~1–2 x 10^{12} N m^{-1}, and we speculate that loading variations are likely the result of tractions imposed at the base of the plate rather than at plate boundaries. Acting together, these tectonic and sub-lithospheric processes triggered the phases of incision and aggradation that created the Finke's unusual intertwined bedrock gorges over a multi-million-year timescale.

1. Introduction

The last decade has seen growing interest in the idea that rivers may encode information about long-term changes in regional topographic gradients induced by deep Earth processes with origins in mantle convection (e.g., Czarnota et al., 2013; Braun et al., 2013). For ancient drainage systems (spanning ~10^7–10^8 yr) there is the potential to record multiple cycles of flow-induced surface deformation that may otherwise leave few geophysical traces in the terrestrial record. A key challenge with unravelling these histories is that topographic responses to mantle processes must be separated from those rooted in the lithosphere such as seismotectonic strain accumulation and flexure, as well as the role of climate change. Recent studies highlight complex spatial patterns of surface deformation experienced by the Australian continent during the past 100 Myr (e.g., Gurnis, 1998; Sandiford, 2007; Czarnota et al., 2013). These include attempts to decipher patterns of vertical motion based on inversion modelling of river longitudinal profiles (e.g., Barnett-Moore et al., 2014; Czarnota et al., 2014). The conclusions remain equivocal because the dynamics of Australian river systems over million-year timescales are poorly constrained and because these studies assume that the contributions of lithospheric processes to fluvial aggradation and/or incision are negligible. While Australia is widely regarded as the archetypal stable continent, it nevertheless hosts examples of Neogene topographic inversion and substantial ongoing intraplate tectonism (e.g., Célérier et al., 2005; Sandiford and Quigley, 2009; Jansen et al., 2013).

* Corresponding author.
E-mail address: jdj@ig.cas.cz (J.D. Jansen).

https://doi.org/10.1016/j.epsl.2022.117456
0012-821X/

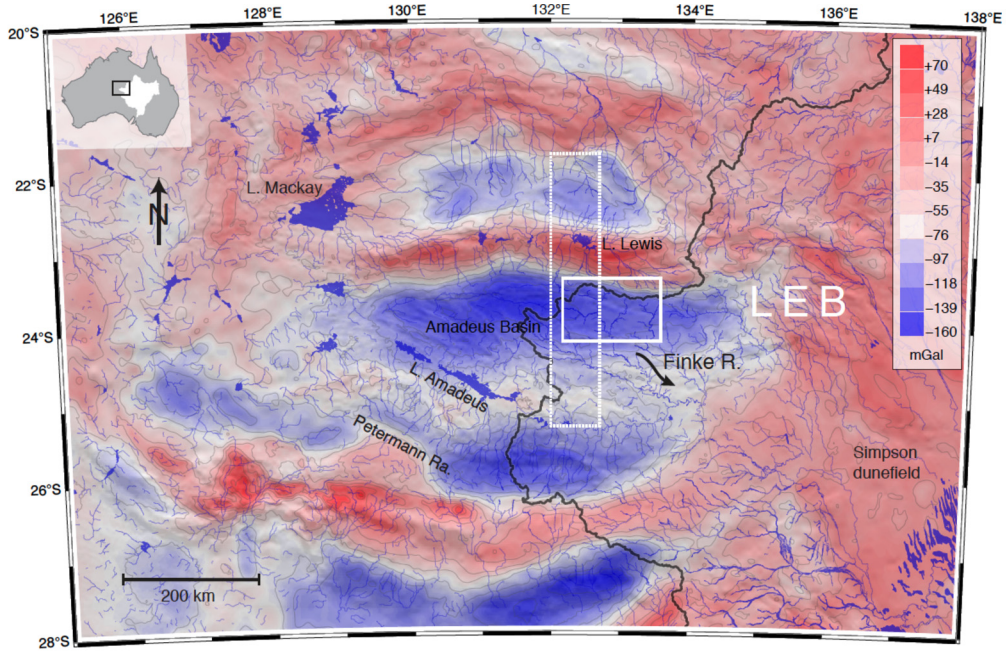

Fig. 1. Complete Bouguer Anomaly gravity map of central Australia. A strong negative gravity anomaly (blue) is focused on the Central Ranges and surrounding area (gravity data from Lane et al., 2020). The white box marks the area shown in Fig. 2A, and the white dashed box (~25.3–21.75° N) marks the location of the gravity swath shown in Fig. 9. The Redbank Thrust Zone corresponds with the northern margin of the Finke catchment, which itself defines the western part of the LEB drainage divide (heavy black line). Note that (1) the western extent of the LEB connects the two most prominent gravity lows along the N- and S-margins of the Amadeus Basin from where the adjacent segments of the LEB divide divert eastward along steep gravity gradients; and (2) in this part of central Australia, streams (blue lines, Crossman and Li, 2015) flow orthogonal to the gravity gradient—away from gravity troughs towards gravity ridges. Top-left inset shows the Australian mainland, map area (black rectangle) and the 1.1 million km^2 LEB (white). The full range in gravity anomaly for the area shown is +67 to −159 mGal. (For interpretation of the colours in the figure(s), the reader is referred to the web version of this article.)

Our understanding of stress in the Australian lithosphere has been well established over the last few decades thanks to field evidence, seismic records and modelling (Coblentz et al., 1995). To first order, the broad pattern of lithospheric stress can be related to the interaction of plate boundary sources of stress together with spatial variations in gravitational potential energy. In central Australia, this imposes NNE-SSW compression expressed, for example, by the 2018 M_W 6.1 Petermann Range earthquake (Attanayake et al., 2020). However, the temporal evolution of the stress field is less resolved. Sandiford et al. (2004) argue that the compressional stress field was established in the Eocene in response to Australia's northward acceleration and that compressional stress has continued to accrue in pace with the resistance to plate motion exerted along convergent plate boundaries (e.g., Papua New Guinea, New Zealand and the Himalaya)—whereas prior to the Eocene the intraplate stress field was largely extensional. Such a framework accounts for a wide variety of seismic and tectonic observations (e.g., Hillis et al., 1997; Jansen et al., 2013), but others have suggested a more varied history. For example, Lubiniecki et al. (2020) show considerably more spatial and temporal variability in the *in situ* stress state than is relatable to far-field plate boundary interactions; they argue that the southern Lake Eyre Basin (LEB) shows signs of a switch from extension to compression as recently as late Pliocene.

The Finke River (or *Larapinta* in the indigenous Arrernte language) in the western LEB is held to be among the most ancient drainage systems on Earth based on its antecedence to fold structures in the Amadeus Basin dating from at least ~300 Ma (Figs. 1 and 2) (Ward, 1925; Madigan, 1931; Mabbutt, 1966; Teyssier, 1985; Haines et al., 2001: see review in Baker, 2021). While such antiquity is speculative, erosion here is unquestionably slow (Wells and Callen, 1986; Belton et al., 2004; Heimsath et al., 2010; Struck et al., 2018a,b). From its present-day headwaters at 1380 m above sea level, the Finke traverses a belt of successive west-east folded strike ridges known collectively as the Central Ranges, flowing ~800 km southeast across the LEB towards Lake Eyre at ~15 m below sea level. As one of the world's largest internally draining, or endorheic basins, the 1.1 million km^2 LEB is enigmatic. Its formation has been attributed to the northward passage of the Australian lithosphere over complex convective structures in the mantle since ~40 Ma (Schellart and Spakman, 2015). However, the notion that the LEB is a dynamically controlled depression that migrates southwards at plate velocity rates of ~70 km Myr^{-1} (Müller et al., 2008) seems fundamentally at odds with the existence of drainage systems that have sustained great antiquity without major reshaping.

While it seems plausible that the Finke encodes information on the spatial and temporal dynamics of mantle flow, other factors also likely impact its form and behaviour. In particular, the Finke's headwaters coincide with a cluster of extreme free-air gravity anomalies that count among the largest preserved within continental interiors globally (Fig. 1). The gravity field in central Australia points to unusually large loads within the lithosphere that are supported elastically (e.g., Lambeck, 1983; Jackson and McKenzie, 2022), the ongoing response to which Beekman et al. (1997) argue has modified regional topography in the Cenozoic. Independently, the continental interior has also experienced a complex climate history involving Pleistocene glacial cycles superimposed on a long-term post-Miocene drying trend (Bowler, 1976; Fujioka et al., 2005).

The gravity anomalies in central Australia date to at least the Palaeozoic intraplate tectonic activity associated with the Alice Springs (~450–300 Ma) and Petermann Range (~550–500 Ma) orogenies (Teyssier, 1985; Beekman et al., 1997; Haines et al., 2001), and may have antecedents linked with the initiation of large intracratonic basins in the Neoproterozoic (Lambeck, 1983). The major structure in the Alice Springs Orogen is the south-verging Redbank Thrust Zone (RTZ), which coincides with a steep gravity

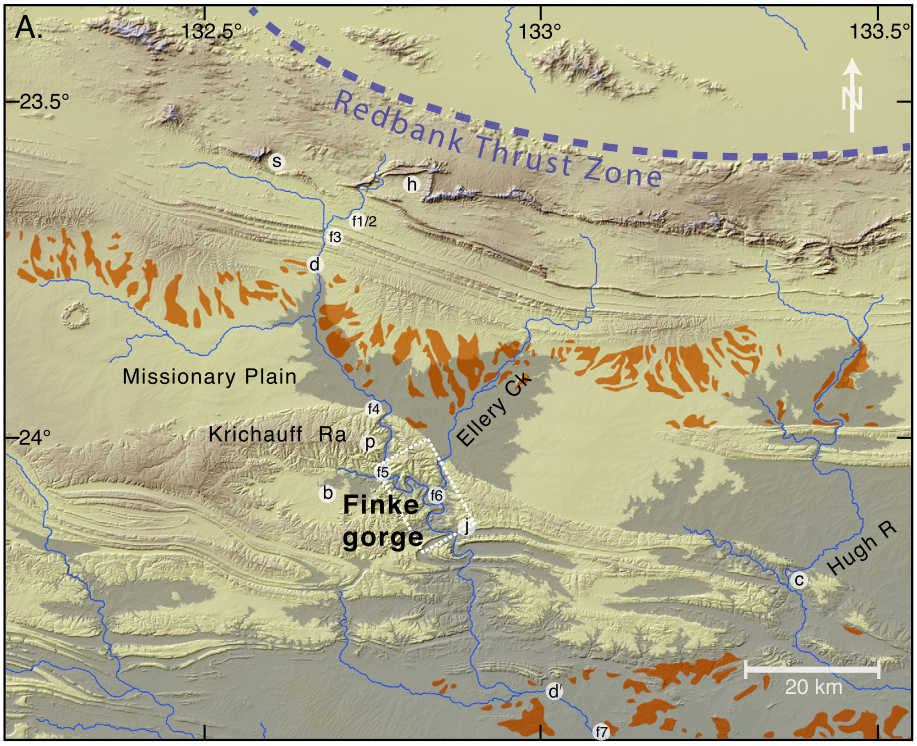

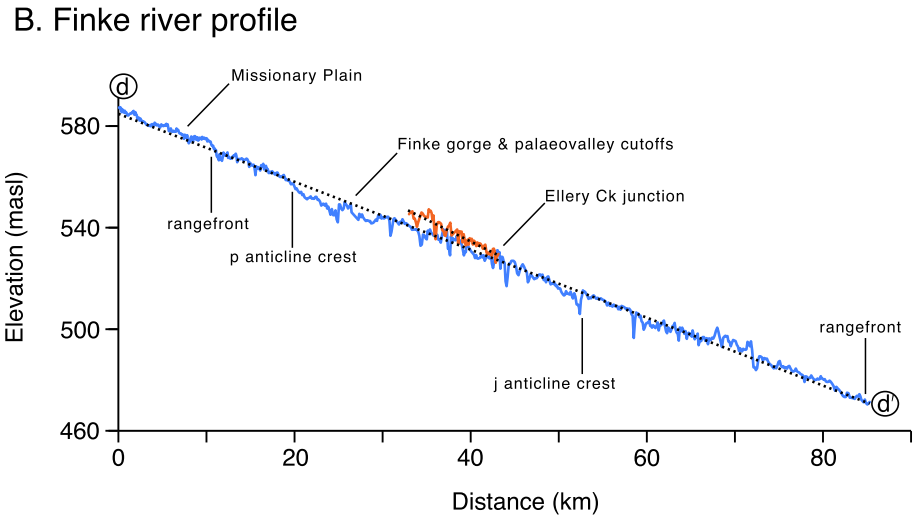

Fig. 2. Central Ranges topography. (A) Topographic hillshade map (SRTM 1-arcsec data, Farr et al., 2007) of the Central Ranges centred on the upper Finke River (drainage area ~4500 km^2 upstream of the Ellery Creek junction) and Redbank Thrust Zone (purple dashes). The areas of low (<614 masl) elevations (dark shading) illustrate the close topographic relationship between Finke's palaeovalley fill and the sediment-mantled pediments and terraces (orange) on Missionary Plain (Mabbutt, 1966; Raymond et al., 2012). Note resistant ridges (h) marking the source of the Heavitree quartzite gravels including: Mt Sonder (s); Palm Valley anticline crest (p); a thin sediment cover west of the gorge within the Palm Valley synclinal basin (b); James Ranges anticline crest (j); and a minor set of palaeovalley cutoffs (c) on the Hugh River. Locations of channel bed samples for ^{10}Be-^{26}Al analysis (f2–f6) are shown (for samples inside gorge, see Fig. 3 outlined by white dashed box); note f7 is shown 22 km upstream of its true position. (B) Longitudinal river profile of Finke Gorge, d–d′ (blue line, see also in panel A), plus Ellery Ck (orange line) near the junction. Linear regression lines (black dashes) fitted to the profiles show the profiles to be overall linear, with average bed slopes of ~1.3 m km^{-1} and ~1.7 m km^{-1} for the Finke and Ellery, respectively. Upstream and downstream rangefronts mark the extent of Finke Gorge incising the folded Amadeus Basin rocks, and the crests of the Palm Valley (p) and James Ranges (j) anticlines are shown.

gradient that separates a prominent gravity ridge to the north and southward trough (Figs. 1 and 2). The gravity high in the hanging wall of the RTZ hosts lower crustal mafic granulites. The gravity-low in the footwall coincides with Missionary Plain, Finke Gorge (Fig. 2), and part of a ~3.7 km thick Devonian foreland basin, the Pertnjara Group. Similar large gravity anomalies are associated with the north-verging Petermann Thrust Zone in the Petermann Ranges some ~300 km further south (Fig. 1).

Several observations imply that the regional geomorphology has been affected by ongoing surface deflections rooted in the gravity anomalies. To first order, the topography is inversely correlated with gravity. Both to the north and south, rivers drain either from headwaters within, or across, gravity troughs towards gravity ridges (Fig. 1). Notably, the western-most limit of the LEB drainage divide forms a meridional-trending limb that connects the most extreme lows in the two gravity troughs along the northern

and southern boundaries of the Amadeus Basin. From there, the drainage divide diverts abruptly eastwards along the steep gravity gradients that bound the Amadeus Basin by some ~250 km in the north and ~100 km in the south. Drainages also converge locally towards endorheic playa systems aligned along gravity ridges (Fig. 1). The long-lived nature of the axial alignment of the topographic lows is reflected in Cenozoic depocentres. For instance, coincident with the gravity high in the hanging wall of the RTZ, the endorheic Lake Lewis Basin (Fig. 1) hosts up to ~150 m of lacustrine sediments dating back to the Mid-Late Eocene (English et al., 2001). The endorheic catchment centred on Lake Amadeus overlies at least 80 m of basin fill (Chen et al., 1993) containing probable Pliocene or older lacustrine sediment. It is likely that Lake Amadeus was formerly integrated with the Finke-LEB; its separation is attributed to surface deformation together with aeolian dune expansion linked to Pleistocene aridity (Lloyd and Jacobson, 1987).

At Finke Gorge, an unusual set of hanging palaeovalley cutoffs signify incision and aggradation of a remarkably high amplitude (up to ~80 m) for a putatively stable tectonic setting. Our aim here is to exploit the Finke's sedimentary archives to uncover a record of surface deformation. To reconstruct the history of events, we measure cosmogenic ^{10}Be and ^{26}Al in fluvial remnants stored in the palaeovalley cutoffs. We then apply a Markov chain-Monte Carlo-based inversion model to test two limiting-case hypotheses proposed to account for the nuclide inventories contained within the sediments. Based on our results we discuss the potential drivers of the Finke Gorge record, building upon some new perspectives on the geodynamics of central Australia and their implications for the origins of the LEB.

2. The Finke palaeovalley

The Finke River forms a sinuous gorge over a 30 km reach where it dissects the Krichauff Ranges and James Ranges with up to 300 m relief (Fig. 2A). Remarkably, this gorge is intertwined with a relict and somewhat less deeply incised gorge that forms hanging junctions, suggesting an epigenetic origin. These palaeovalley cutoffs have been noted previously (Mabbutt, 1966; Pickup et al., 1988; Baker, 2020), yet the unusual overprinting of the two gorges remains unexplained. The hanging cutoffs occur mainly upstream of the Ellery Creek junction on both the Finke and the Ellery (Fig. 3) corresponding to a broad syncline (Fig. 2). The palaeovalley floors are lined with gravel piles up to several metres thick comprising locally derived Hermannsburg (Devonian) sandstone clasts along with well-rounded quartzite (strictly, silicified sandstone) clasts traceable to the Neoproterozoic Heavitree Formation, which caps the highest elevations (Mt Sonder, 1380 masl) ~50 km upstream (Fig. 2A). Basal exposures reveal that the gravels form partially disintegrated conglomerate remnants (>3 m thick) locked together by a mix of siliceous and ferruginous cement. Although highly resistant, the Heavitree quartzite clasts are frequently found broken into angular fragments, implying long-term residence in the palaeovalley. A less developed and more alluviated set of intertwined valleys occurs where the Hugh River also crosses the James Range (Fig. 2A), although we did not examine that site.

Two key observations provide clues to the origin and evolution of the palaeovalleys: 1) as well as lining the Finke's channel bed, Heavitree quartzite gravel is strewn across a broad bedrock shoulder ~80 m above the cutoffs (Pickup et al., 1988); and 2) neither of the intertwined gorges show traces of lateral meander migration, such as strath terraces or steps on the concave bends. From this we surmise that the Finke valley was up to ~2.5 km wide prior to incision of the palaeovalley (*Incision 1*). Much later, the lateral switch from the palaeovalley to the new course implies valley-floor alluviation (40–60 m), which blanketed entirely the shoulder surface and bedrock meander cores followed by carving (*Incision 2*) of the ~200 m wide epigenetic gorge that is active today (Figs. 3 and 4).

3. Methods and results

3.1. Morphology of the cutoffs

We analysed the morphometry of the epigenetic gorge and sixteen palaeovalley cutoffs using 10 m grid-resolution digital elevation data derived from synthetic aperture radar (TOPSAR) produced by NASA in 1996 and 2000. The longitudinal profiles for both gorges were constructed after reducing the noise in the TOPSAR data (see details in Supplementary Data S3). Given that each bedrock meander core was necessarily overtopped by fluvial gravels at the time of lateral channel shift, the height of the bedrock between these two gorge systems represents a minimum former thickness of gravel that once filled the palaeovalley (Figs. 3B and 4). An envelope line fitted to the highest bedrock meander cores pins the minimum level of alluviation at ~614 masl.

Reconstructing the palaeovalley longitudinal profile is not straightforward because bedrock is rarely exposed and the elevation of gravel pile remnants in each cutoff is more a function of incomplete sediment flushing than of the former channel bed level. As some cutoffs are lower in elevation (i.e., c3, c7, c9, c15, c16; Fig. 3), the profile varies considerably. Applying linear regression to elevations along the intertwined gorges (c1 to c10), we find that the average slope of the channel bed and palaeovalley overlap within 95% confidence intervals: 0.83–1.02 m km^{-1} and 0.85–1.71 m km^{-1}, respectively (Fig. 3B). Their channel width and sinuosity are also alike (Fig. 3), as is their dominant bedload size-fractions of pebbles and cobbles (channel width and grain size is based on visual comparison only). These observations suggest that the old and new gorges were both shaped by similar discharge and sediment load regimes. The fluvial incision possibly involved knickpoint retreat, but any former knickpoints (if they did exist) have long diffused away. The Finke's long profile is remarkably linear for ~85 km from Missionary Plain and across the folded Amadeus Basin sequence at a slope of ~1.3 m km^{-1} (Fig. 2B).

3.2. Cosmogenic nuclide analysis and results

In situ-produced cosmogenic radionuclides (e.g., ^{10}Be and ^{26}Al) accumulate in minerals within the upper few metres of Earth's surface, due to exposure to secondary cosmic rays, and are lost via erosion and radioactive decay (Lal, 1991). The metre-scale penetration depth of nuclide production means that the integration timescale varies inversely with erosion rate. For cosmogenic ^{10}Be-^{26}Al analysis, we collected amalgamated samples (1–3 kg, 14–22 clasts) of Heavitree quartzite gravels (~30–100 mm intermediate-axis) from the highest remnant gravel deposits in seven of the palaeovalley cutoffs and at two channel bed sites (f5 and f6; Fig. 3) (Supplementary Table S1). In addition, one sample (c11) was collected from fluvial gravels capping a local hilltop. After crushing, quartz purification and Be and Al extraction were conducted on the 0.25–0.5 mm size fraction at the Australian Nuclear Science and Technology Organisation following standard methods of HF/HNO$_3$ (Kohl and Nishiizumi, 1992), hot phosphoric acid (Mifsud et al., 2013), and ion chromatography (Child et al., 2000). Be and Al isotope ratios were measured on the Sirius accelerator mass spectrometer (Wilcken et al., 2019) and normalised to standards KN-5-2 (Be) (Nishiizumi et al., 2007) and KN-4-2 (Al) (Nishiizumi, 2004) (Supplementary Table S2).

The palaeovalley samples contain between ~0.5 and 1.9 million ^{10}Be atoms g^{-1}. A two-nuclide plot (Fig. 5) is the conventional

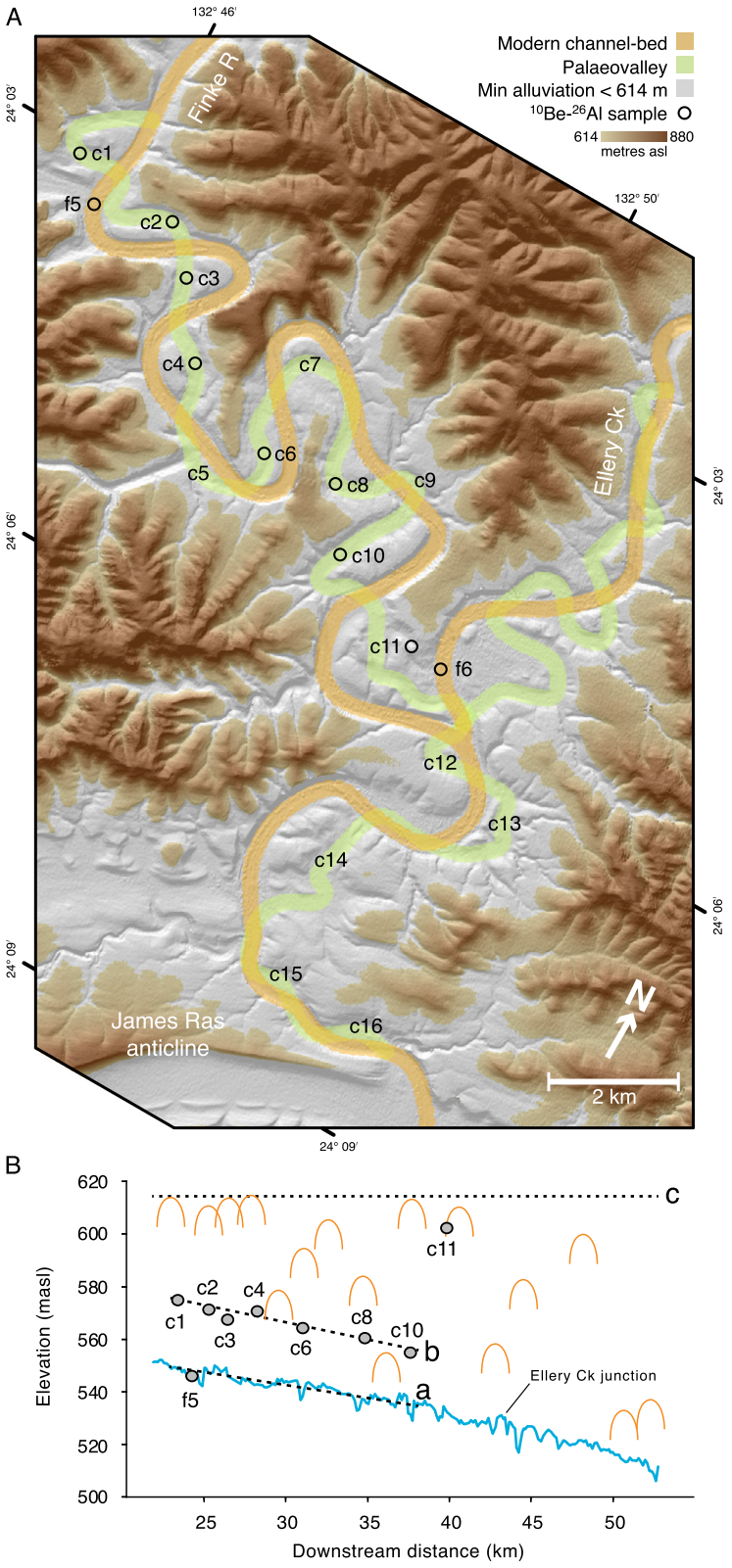

Fig. 3. Intertwined epigenetic and palaeovalley gorges. (A) Intertwined epigenetic (*Incision 2*) and palaeovalley (*Incision 1*) gorges of the Finke River and lower Ellery Creek (flow downpage) on a topographic hillshade map (TOPSAR). Shown are the 16 palaeovalley cutoffs (c1–16) along the Finke and sites sampled for ^{10}Be-^{26}Al analysis (open circle), including the channel bed (f5, f6). Both channel sinuosity (i.e., ratio of channel length to straight line length, calculated as 2.15 in the present-day gorge and 2.16 in the palaeovalley) and channel width are essentially equivalent for the two systems. Areas previously blanketed by sedimentary fill (grey shade), enabling lateral channel migration, are shown topping bedrock meander cores and shoulder surfaces (<614 m). At the base of the map, the two gorges converge where they meet the breached limb of the James Range anticline; the crest of the Palm Valley anticline crosses the Finke close to the map's upstream limit. (B) Longitudinal profiles of the Finke Gorge channel bed (cyan) relative to the palaeovalley cutoffs sampled for ^{10}Be-^{26}Al analysis (grey-filled circles); the extent matches panel A. Note sample c11 is from hilltop fluvial gravels. Average bed slopes (with 95% confidence intervals) are (a) Finke Gorge, 0.83–1.02 m km^{-1}, and (b) palaeovalley cutoffs, 0.85–1.71 m km^{-1}. The elevation of each bedrock meander core (apex of orange arch) is shown for the 16 cutoffs. A surface (c) fitted to the highest meander cores (~614 masl) defines the estimated minimum level of alluviation. Elevations (in metres above sea level) are based on TOPSAR digital elevation data; downstream distance is matched to that in Fig. 2B.

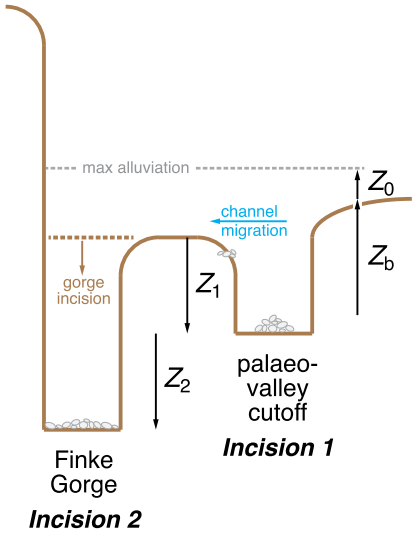

Fig. 4. Schematic valley section. Finke Gorge (*Incision 2*) and palaeovalley (*Incision 1*) are shown here separated by a bedrock meander core of height, Z_1, which defines the minimum gravel-pile thickness to allow lateral channel migration. Samples for ^{10}Be-^{26}Al analysis were collected from gravel-pile crests in the palaeovalley at minimum burial depth, Z_b, below the extrapolated upper gravel surface (Fig. 3). To this minimum burial depth, is added an unknown sediment thickness, Z_0, of up to 20 m. All shown at ~10-times vertical exaggeration.

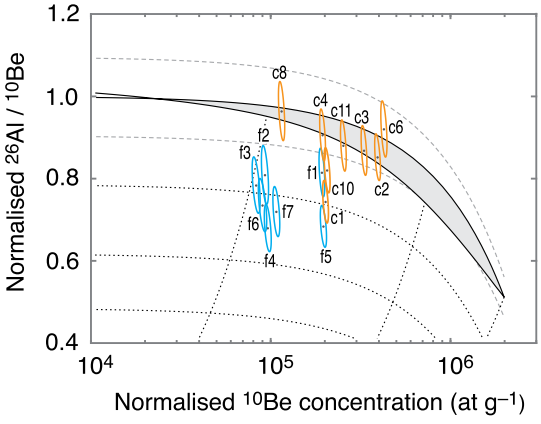

Fig. 5. Two-nuclide ^{10}Be-^{26}Al plot. Two-nuclide plot of paired ^{10}Be-^{26}Al data normalised to reference production rates (Expage-201902 calibration dataset; https://expage.github.io) for ^{10}Be (4.05 ± 0.21 at g^{-1} y^{-1}) and ^{26}Al (28.02 ± 2.25 at g^{-1} y^{-1}), showing ±1 σ uncertainty in 8 palaeovalley samples (orange ellipses: c1–c11) and 7 channel bed samples (cyan ellipses: f1–f7) upstream, within, and downstream of the gorge (note samples f2, f3, f4, f6, f7 are recalculated from Struck et al., 2018b). The steady-state erosion island (grey fill) includes ±1 σ production rate uncertainties (long-dash grey lines). We note that representing ^{10}Be-^{26}Al data in a two-nuclide plot assumes a steady exhumation rate, as in scenario *A*; hence this plot is not valid for scenario *B*.

method of analysing nuclide inventories in samples with a simple history of exhumation and burial. This demands strictly that samples experienced steady bedrock erosion at their source and were then transported and buried with no intermediate storage. The ^{26}Al-^{10}Be data fall across and below the steady-state erosion island (Fig. 5). The palaeovalley gravels mostly fall on the island and tend to have higher ^{10}Be abundance and higher ^{26}Al/^{10}Be ratio relative to the channel bed samples. This difference is in part a function of grain size. Five bed samples (f2, f3, f4, f6, f7) include only sand-sizes, whereas the palaeovalley samples (plus f1 and f5 from the channel bed) include only gravels. The effect of grain size is seen most clearly in f1 and f2 collected from the same channel bed locality in the Finke headwaters: f1 (gravels) contains double the ^{10}Be abundance of f2 (sand). The low ^{26}Al/^{10}Be ratios

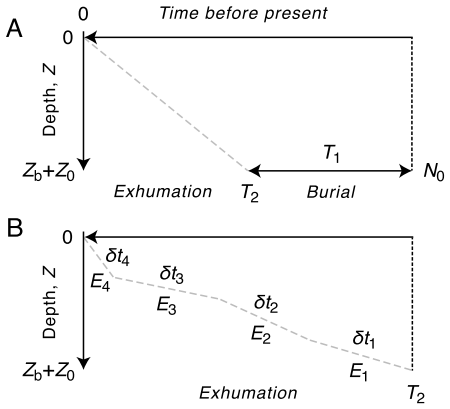

Fig. 6. MCMC inversion model parameters illustrating scenarios *A* and *B*. Schematic plots of gravel-pile depth versus time, with the upper-left origin representing the present-day surface, and model parameters: initial concentrations of ^{10}Be and ^{26}Al, N_0; period of burial within the gravel-pile, T_1; onset of sample exhumation, T_2, and sample burial depth, $Z_b + Z_0$ (see main text). (A) Gravel-pile depth versus time for scenario *A*, showing steady exhumation path. (B) Gravel-pile depth versus time for scenario *B*, showing exhumation paths parameterised with four linear segments of differing exhumation rate (E_1 to E_4) over four sequential time intervals (δt_1 to δt_4) (see main text).

measured in the f5 channel bed gravels could be the result of long-term burial within mantled pediments on Missionary Plain, but f1 lies upstream of any major sediment storage (Fig. 2A). Alternatively, the low ^{26}Al/^{10}Be ratios may be caused by rapid, non-steady exhumation via (for f5) deep gullying on Missionary Plain feeding buried clasts directly into the Finke; and (for f1) episodic (coseismic?) rockfall activity on steep quartzite ridges in the RTZ. We note that the steady-state erosion island and the burial isochrons (Fig. 5) are computed using surface production rates and are therefore not valid for f1 and f5, if those samples derive from depth.

Treating the nuclide abundances in the palaeovalley gravels as apparent exposure ages would severely underestimate the age of the gravel piles, because a simple exposure-burial trajectory cannot reproduce the ^{26}Al-^{10}Be inventories in the palaeovalley from those in the present-day channel bed. Instead, the palaeovalley nuclide inventories are likely the outcome of a complex history involving burial and exhumation for which we consider a couple of scenarios below.

3.3. Inversion modelling with cosmogenic nuclides

The cosmogenic nuclide inventories measured in the palaeovalley gravels are a function of their erosion history in the sediment source area, their exposure on hillslopes and in streams during transport and their burial/exhumation in the palaeovalley. We propose two limiting-cases (while acknowledging that reality may have combined aspects of both), as given below.

(*A*) A relatively short burial-exhumation scenario allied with steady erosion of the gravel piles during incision of the epigenetic gorge. Here, some fraction of the pre-burial nuclide inventory is preserved in our samples, and deep within the gravel piles the ^{26}Al/^{10}Be ratio declines with time because ^{26}Al decays faster than ^{10}Be (Fig. 5). We parameterise this model (Fig. 6A) using initial concentrations of ^{10}Be and ^{26}Al (N_0); the period of burial within the gravel-pile (T_1); and the onset of sample exhumation from burial within the deposit (T_2). A steady exhumation rate is assumed from T_2 to the present.

(*B*) A long burial-exhumation scenario whereby erosion of the gravel piles can be steady or non-steady. Here, burial has been sufficiently long and deep to effectively erase the pre-burial nuclide inventory via radioactive decay (>3–7 Myr of burial reduces the inventory to <5% assuming a catchment-averaged erosion rate

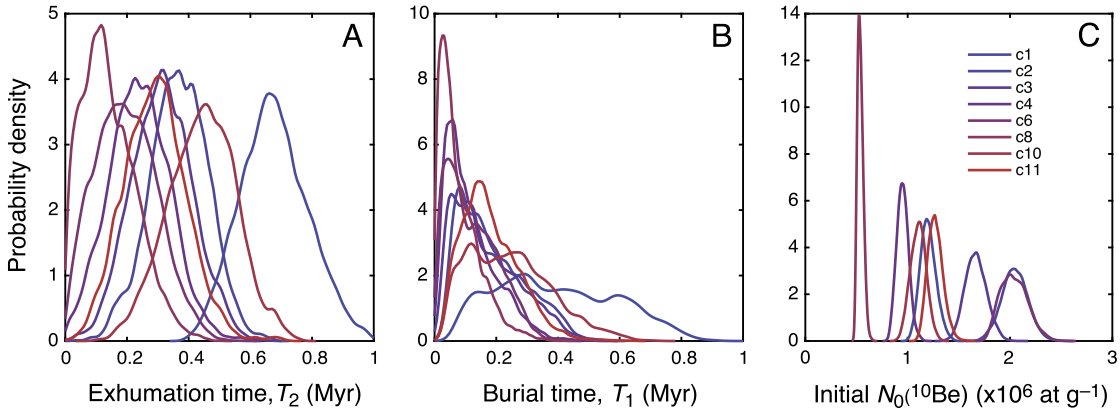

Fig. 7. Probability distributions for 8 samples computed by the MCMC inversion model (scenario *A*). (A) Timing (T_2) of onset of sample exhumation to the gravel-pile surface; (B) burial period (T_1) within gravel pile; and (C) initial ^{10}Be concentration at time of deposition within the palaeovalley.

of 5.0 ± 2.4 mm kyr^{-1}; see Supplementary Table S2). Samples start with zero nuclides within the gravel pile and a new inventory arises during steady or non-steady exhumation, hence variation in ^{26}Al/^{10}Be ratio can also be explained by samples accelerating to the surface (Knudsen and Egholm, 2018). We parameterise the exhumation paths via eight free parameters (Fig. 6B) that describe four linear segments of differing exhumation rate (E_1 to E_4) over four sequential time intervals (δt_1 to δt_4). The total exhumation timescale is limited to 10 Myr.

To test whether our interpretations agree with the nuclide inventories and to constrain the model parameters involved, we apply a Markov chain-Monte Carlo-based (MCMC) inversion model to the paired ^{10}Be-^{26}Al data (n = 8). This entails a system of forward models that compute iteratively the ^{10}Be and ^{26}Al abundances subject to variations in model parameters followed by inversion (Knudsen et al., 2015). For both scenarios *A* and *B*, a minimum burial depth (Z_b) is computed from the sample elevation below the extrapolated upper gravel surface at 614 masl (Figs. 3 and 4). To this minimum burial depth, we add a random sediment thickness (Z_0) of up to 20 m to accommodate the possibility of a somewhat deeper valley fill. All model parameters are allowed to vary between samples except the common parameter Z_0. The simulations deploy 4 random walkers, each performing 120,000 iterations, and the model acceptance ratio is 0.25–0.35 (Knudsen et al., 2015). Nuclide production rate scaling (Stone, 2000) was adopted with reference spallogenic production rates of 4.05 ± 0.21 atoms g^{-1} yr^{-1} (^{10}Be) and 28.02 ± 2.25 atoms g^{-1} yr^{-1} (^{26}Al) taken from the Expage-201902 calibration dataset (https://expage.github.io). All computations assume a ^{10}Be half-life of 1.387 Myr (Chmeleff et al., 2010; Korschinek et al., 2010) and ^{26}Al half-life of 0.705 Myr (Nishiizumi, 2004).

3.4. Inversion modelling results

Fig. 7 shows the MCMC inversion modelling outputs for the 8 sample pairs pertaining to the short burial-exhumation case (scenario *A*). Note that the interval of exhumation (T_2) generally exceeds that of burial (T_1), and histories ($T_1 + T_2$) cluster chiefly within the past 1 Ma. According to this scenario, alluviation and burial spanned generally <0.5 Myr (or up to ~0.9 Myr for c1). Gravel-pile exhumation (Fig. 7A) and incision of the epigenetic gorge (*Incision 2*) was initiated after ~0.7–0.6 Ma (or as early as ~1 Ma for c1).

Fig. 8 shows the modelled exhumation pathways pertaining to the long burial-exhumation case (scenario *B*). Owing to the attenuation of cosmic rays with depth, the deeper modelled pathways (further back in time) are less well constrained relative to upper levels in the profile. Most samples yield an abundance of models with essentially linear (steady) exhumation to the surface, but especially for sample c1 there is an abrupt acceleration in the upper 1–2 m.

4. Sedimentary archives in the Finke drainage system

Our interpretation of the nuclide inventories in the palaeovalley gravels builds directly on the two burial-exhumation scenarios tested above and affords the following arguments.

(1) In scenario *A*, burial must be relatively recent and short-lived (<800 ka and mostly <200 ka; Fig. 7). Burial in the gravel piles was sufficiently short to partially retain pre-burial nuclide inventories from the sediment source area. However, the requirement to both fill the palaeovalley and incise the epigenetic gorge within the past ~1 Ma demands rates of activity that seem improbably fast given the ridges supplying the Heavitree quartzite gravels erode slowly (i.e., 8 samples yield erosion rates spanning ~0.16–2.8 mm kyr^{-1}; Supplementary Tables S1 and S2). Further, the highly weathered state of the quartzite clasts we sampled suggests much longer (>1 Myr) burial in the gravel piles. Carving the ~60–80 m deep epigenetic gorge after ~0.7–0.6 Ma implies an average bedrock incision rate of ~86–133 mm kyr^{-1}. This rate is exceptionally fast for a river that mobilises its coarse bedload once per decade or less (Pickup et al., 1988), and it greatly exceeds the most probable bedrock fluvial incision rate (11–24 mm kyr^{-1}) of another large LEB river, Cooper Creek (Jansen et al., 2013).

(2) The nuclide inventories of the palaeovalley gravels cannot be reconstructed without a complex history of burial and exhumation, which appears to have decoupled them from their source. Accordingly, we favour circumstances closer to the long term burial-exhumation of scenario *B*. In attributing low ^{26}Al/^{10}Be ratios to non-steady exhumation, we envisage some samples were held at a few metres depth in the gravel piles for intervals exceeding 1 Myr followed by acceleration to the surface (e.g., via gullying) within the past few hundred thousand years (Fig. 8). This scenario assumes erasure of the nuclide memory during long-term (>3–7 Myr) burial, which means that the timing of either palaeovalley filling or gravel-pile erosion cannot be constrained. That said, exhumation of samples in the gravel pile probably occurred <6 Ma according to a large fraction (P > 0.01) of the accepted models (Fig. 8).

We emphasise that our two model scenarios are designed as limiting cases only. We cannot rule out, indeed it is likely, that reality mixed aspects of both scenarios *A* and *B*. For instance, non-steady erosion of the gravel piles in combination with survival of some fraction of the pre-burial nuclides. The upshot is that the upper Finke has sustained alternating phases of incision–

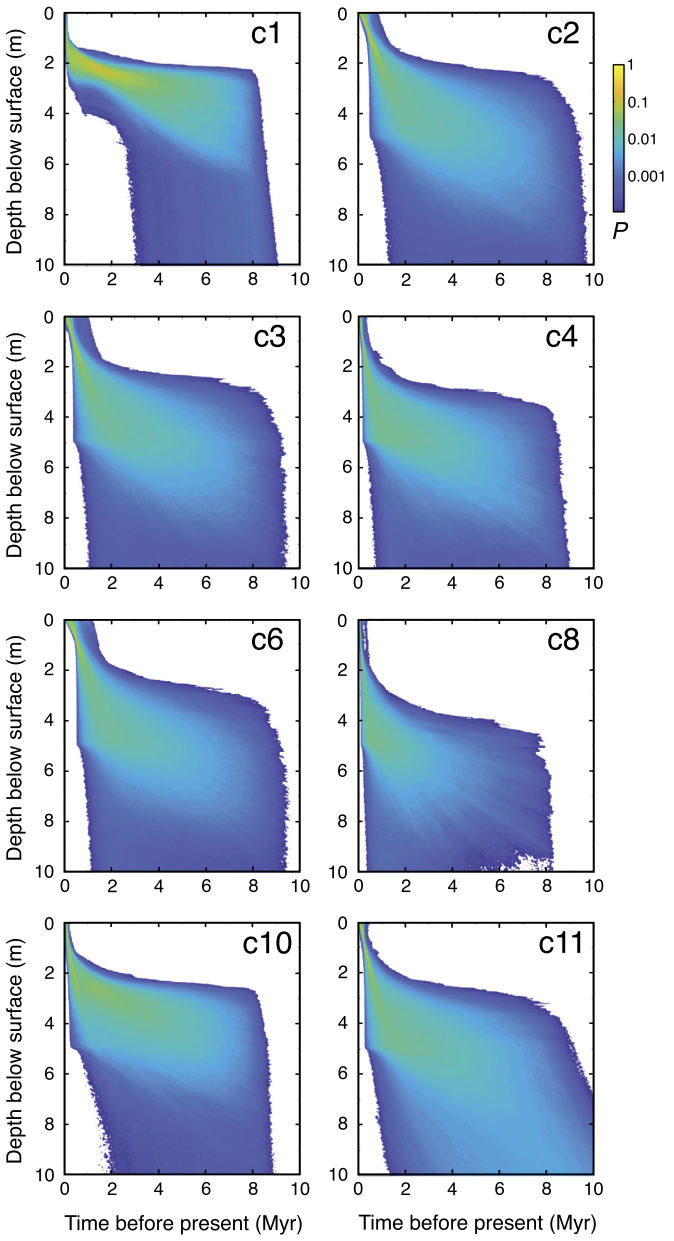

Fig. 8. Exhumation pathways for 8 samples computed by the MCMC inversion model (scenario *B*). Modelled pathways through the upper 10 m of exhumation to the gravel-pile surface; *P* is normalised probability density and ~160,000 simulations are shown.

aggradation–incision probably over a million-year timescale. In the following we consider the possible mechanisms responsible.

5. Discussion

We set out to investigate processes responsible for the distinctive intertwined bedrock valleys of the Finke, with the aim of using geomorphology to quantify deformation across central Australia more broadly. We have outlined a geomorphic history of the Finke beginning with a predominantly alluvial river that crossed the Krichauff Ranges in a broad valley up to 2.5 km wide. A shift to erosion (*Incision 1*) then cut a sinuous bedrock gorge 40–60 m deep (i.e., the palaeovalley) followed by aggradation that buried the palaeovalley under a thick cover. A second incision phase (*Incision 2*) then cut a ~60–80 m deep epigenetic gorge, leaving ~20 m-high hanging junctions with the exhumed palaeovalley. Two aspects are striking in the context of central Australia: the amplitude of the fluvial incision-aggradation, and the magnitude of the shifts in sediment transport capacity implied by the switch between incision and aggradation. Here we consider explanations for the incision-aggradation record, beginning with what previous workers have considered to be a strong driver of landscape evolution in central Australia: late Cenozoic climate change.

5.1. A role for climate?

Climate influences the sediment transport capacity of rivers mainly via rainfall. Palaeoclimate analyses of terrestrial and marine stratigraphy, including macro- and microflora fossils (e.g., Wells and Callen, 1986; Alley, 1998), indicate a far wetter early and middle Cenozoic relative to today. Australia's northward drift, together with the global cooling trend since the mid-Miocene, has culminated in intensified aridity in central Australia from ~4–2 Ma (Bowler, 1976; Fujioka et al., 2005). Long-term aridification in the Finke may be seen in the shift from iron to carbonate enrichment in the mantled pediments on Missionary Plain (Fig. 2A), which comprise a partly iron-cemented high terrace, a middle terrace with leached red-earth soils, and a low terrace with locally calcreted gravels (Mabbutt, 1966). The upper two of three mantled pediment levels are correlated with the Finke palaeovalley fill (Mabbutt, 1966), tentatively implying a pre-Quaternary age. Future efforts to date the pediment mantles would be well spent.

Climate surely contributed to incision and aggradation along Finke Gorge, but we consider it a secondary control for several reasons. First, the essentially identical morphometry of the palaeovalley and epigenetic gorge (in terms of width, sinuosity and bedload calibre) argues for a comparable discharge regime, and this does not concur with long-term aridification. Second, the amplitude of bedrock incision (~40–80 m) during the two gorge incision phases exceeds what could plausibly be achieved in a 100-kyr glacial-interglacial climate cycle. Given the expected maximum fluvial incision rate of a few tens of mm kyr^{-1} (Jansen et al., 2013), only a small fraction of the epigenetic gorge depth could be incised during a 100 kyr cycle (and cycles shortened to 41 kyr prior to ~1 Ma). And third, the unique character of Finke Gorge points to a response restricted locally, rather than the broadscale regional response that would accompany climate change.

5.2. Gravity and topography in central Australia

Finke Gorge coincides with the most extreme gravity anomaly within the Australian continent. The requirement for elastic support of the gravity anomalies in central Australia has been known for decades (e.g., Lambeck, 1983, 1984). Jackson and McKenzie (2022) explore how the density anomalies are supported by a stress regime in the elastic layer of ~30 km effective thickness and ~240 km wavelength, consistent with the distribution of occasional intraplate seismicity (e.g., Attanayake et al., 2020). They emphasise that this regime must necessarily result in normal stress on the lower boundary of the elastic layer "constant and equal to the lithostatic pressure" (p. 7), and they then consider the dynamics that would suppress uplift of the gravity troughs and subsidence of the highs. However, the observation that gravity anomalies align with drainage patterns in the western LEB (Fig. 1) raises an outstanding problem. Beekman et al. (1997) points to the persistent Cenozoic depocentres coinciding with the gravity ridge in the hanging wall of the RTZ, and elsewhere (see Fig. 9A). From this, they argue that in-plane far field compression produces "a stress-amplified downward flexure" (p. 223) at the gravity ridges (e.g., lakes Lewis and Amadeus, Figs. 1 and 9A).

The lithospheric response to in-plane loads is sensitive to the elastic parameters that govern flexure, including the possibility

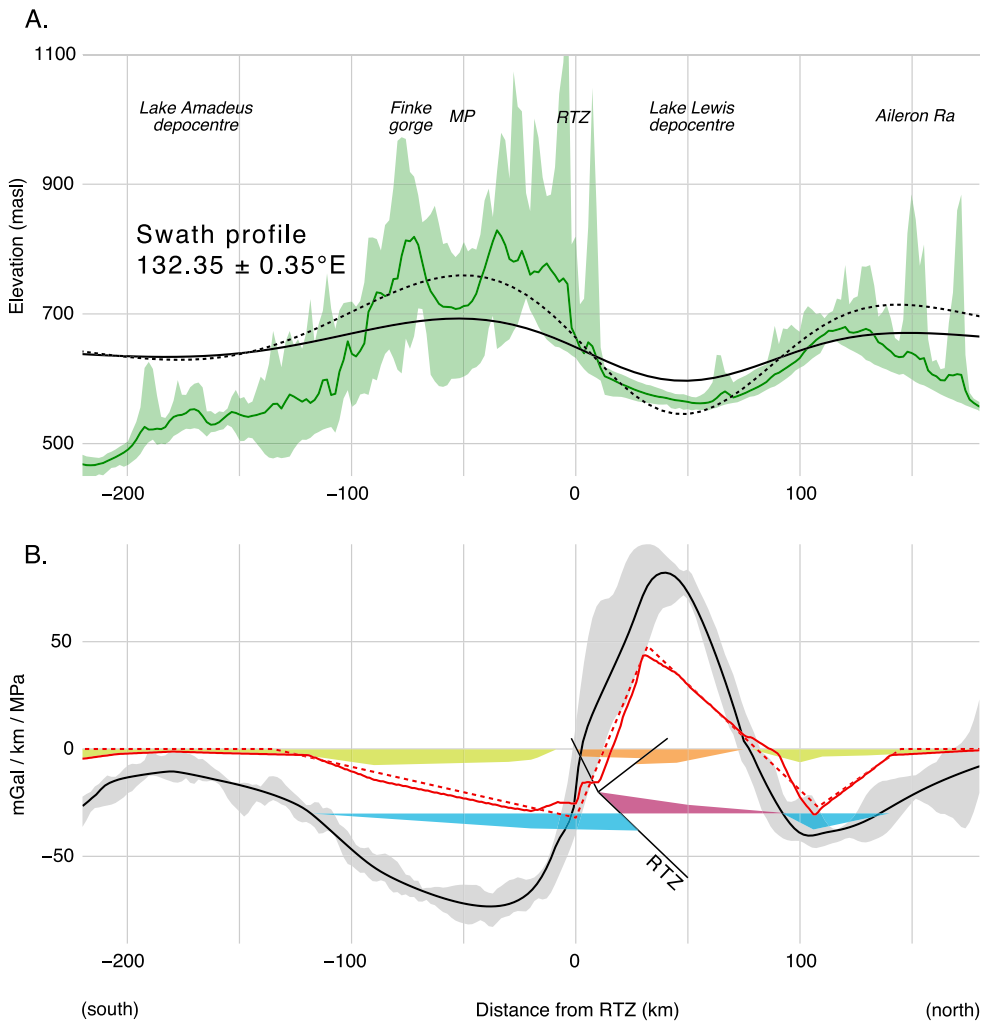

Fig. 9. Topography and simplified gravity model of the study area. (A) South to north topographic swath (132.35 ± 0.35°, ~70 km width, see Fig. 1), showing maximum-minimum (pale green band) and mean (dark green line) elevations plotted with distance relative to Redbank Thrust Zone, RTZ (swath is *X*–*X*′ in Fig. 1). Modelled flexural responses to in-plane loading of 1 x 10^{12} N m^{-1} accompanied by reductions in T_e of 10% (black line) and 20% (black dashes) (see Fig. 10). Topographic forms are labelled (MP—Missionary Plain); note the elevation swath excludes the 1380 m peak, Mt Sonder. (B) Summary of gravity model and vertical loads used to compute flexural response. Vertical scale represents gravity (mGal), crustal depth (km), and vertical loading (MPa). Complete Bouguer Anomaly gravity swath in mGal (grey band) (Lane et al., 2020). Density anomalies are shown as coloured polygons: green—footwall foreland basin (density anomaly −110 kg m^{-3}); cyan—depressed footwall Moho (-350 kg m^{-3}); plum—elevated hanging wall Moho (350 kg m^{-3}); orange—elevated hanging wall lower crust (310 kg m^{-3}), including exposed mafic granulites; RTZ—Redbank Thrust Zone (thin black line). Computed gravity profile (black line, in mGal) and vertical stress (red line, in MPa). Note the flexural response calculated in Fig. 10 uses a simplified vertical stress illustrated by red dashes.

that the effective elastic thickness (T_e) is diminished by in-plane loading (e.g., McNutt and Menard, 1982). To further examine the role of flexure in light of observations at Finke Gorge, we explore the impact of in-plane loading on topographic relief in the presence of vertical loads for both constant and variable T_e. We apply the modelling code of Hindle (2021) to compute topographic responses to small variations in in-plane load and T_e in the presence of vertical loads consistent with central Australia's gravity field (Figs. 9 and 10). In keeping with the insights of Beekman et al. (1997), in-plane loading produces broad low-amplitude anticlines above gravity troughs while synclines develop over gravity ridges. The surface deformation, or flexural relief, is sensitive to both T_e and the magnitude of the in-plane loading (Fig. 9). For a fixed T_e of ~20–30 km, the characteristic response wavelength of flexural relief is 210–260 km, matching key field observations. For example, at $T_e = 30$ km, flexural relief inflexion points correspond approximately to the location of the main topographic forms. At $T_e = 10$ km, the wavelength reduces to ~150 km, which is too condensed relative to the observed topography. For an in-plane load of 1 x 10^{12} N m^{-1}, the flexural relief at $T_e = 30$ km is 6 m, increasing to 19 m at $T_e = 20$ km, and 86 m at $T_e = 10$ km. A 10-fold increase in the in-plane load (to 1 x 10^{13} N m^{-1}) raises the flexural response also by ~10 fold. While this is consistent with observed relief, we consider that such large in-plane loads are implausible, as they would result in stress differences of order 1000 MPa.

Various authors (e.g., McNutt and Menard, 1982; Lowery and Smith, 1995) note that a growing in-plane load should lead to reductions in T_e because of the way stress dependant yield surfaces differentially truncate the elastic core of the lithosphere. Burov and Diament (1995) show an in-plane compression of 4 x 10^{12} N m^{-1} equates to a 20–30% reduction in T_e. Fig. 10B reveals that for the vertical loading pattern considered here, a 10% reduction in T_e (consistent with in-plane load of 1–2 x 10^{12} N m^{-1}) will produce an observable topographic response. Reducing by 10% an initial T_e of 30 km yields 96 m of flexural relief, with an asymmetry and wavelength that approximates the pattern of inferred flexural topography across the RTZ (Fig. 9A). The crucial insight arising from our computations (summarised in Fig. 10) is that when $T_e = 30$ km the flexural response to T_e reduction is an order of magnitude larger than the direct response to in-plane loading.

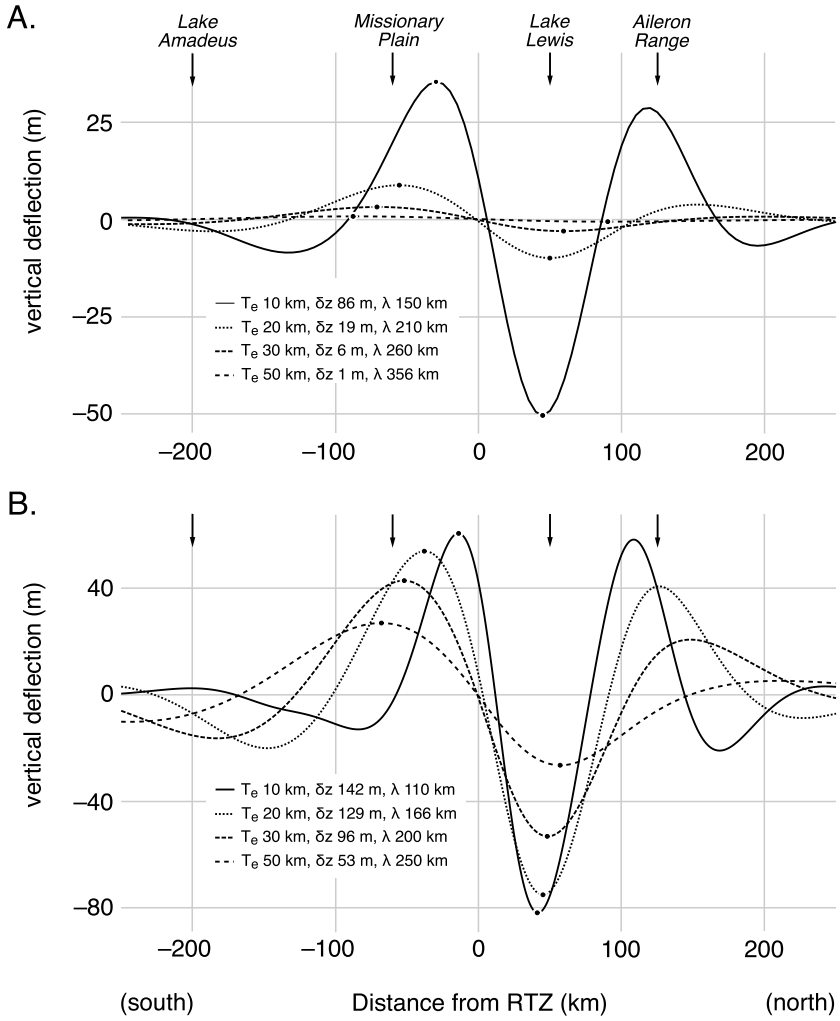

Fig. 10. Modelling flexural response. (A) Flexural topographic response to an in-plane load of F = 1 x 10^{12} N m^{-1} applied to a lithosphere of fixed T_e (10, 20, 30, 50 km) subject to vertical loads (shown by red dashes in Fig. 9B). (B) Flexural topographic response to a 10% reduction in T_e applied to a lithosphere with initial T_e (10, 20, 30, 50 km) subject to vertical loads (shown by red dashes in Fig. 9B). Flexural response is calculated using a numerical solution to the flexure equation documented by Hindle (2021). Distance is relative to Redbank Thrust Zone. Relevant topographic forms are labelled.

5.3. Dynamic flexural response in central Australia

The fluvial incision at Finke Gorge has occurred apparently in the absence of significant coeval, localised faulting, and seems at odds with the slow erosion suggested by published cosmogenic nuclide data (e.g., Heimsath et al., 2010; Struck et al., 2018a). And yet, given that the slowest and therefore longest-reaching ^{10}Be-derived erosion rates integrate back to a maximum of ~2–3 Ma (Struck et al., 2018b), tectonic quiescence in central Australia cannot be assumed to extend beyond the Quaternary. Although no timing is specified, Mabbutt (1966) invokes southward tilting of the Finke drainage system to account for dissection of the mantled pediments on Missionary Plain and to the south (Fig. 2A). Prior to incision, the pediments were graded to the cover that blanketed the palaeovalley and the adjoining synclinal fill west of the gorge (Fig. 2A)—a substantial volume of sedimentary storage of order 10^7 m^3 (assuming a prismatic geometry). We link Mabbutt's southward tilting (steepening) to a boost in stream power that triggered incision of the Finke's epigenetic gorge (*Incision 2*). Related incision extended downstream where pediment fragments stand up to 60 m above the Finke channel (Fig. 2A). Sediments mobilised by the base level fall were cast into the fluvial-aeolian sand plain that extends beyond the ranges for ~200 km before merging with the Simpson dune field (Fig. 1).

As noted by Beekman et al. (1997), the recent geological history of subsidence in the hanging wall of the RTZ suggests evolving, flexurally mediated support. Here we extend that observation to include the alternating incision and aggradation recorded at Finke Gorge, consistent with a cyclical fluvial response (of ~100 m amplitude) over the past few million years. In the previous section, we simulated flexural relief of order 100 m with a ~10% change in T_e for an in-plane loading of 1–2 x 10^{12} N m^{-1} (Burov and Diament, 1995) and reference $T_e = 30$ km (Fig. 10). During loading, such a response tilts and steepens the Finke in the vicinity of the gorge, causing fluvial incision and unloading that drives erosion of the flexural relief and supplies sediment to the gorge.

Previous T_e estimates for central Australia span <10 km to >100 km—see discussion by Kirby (2014) and McKenzie (2015). The uncertainty can be attributed in large part to the low spectral power of Australian topography and its lack of coherence with gravity at the longest wavelengths, which stymies the main estimation methods. While the long term support of large loads suggests considerable finite elastic strength, T_e is everywhere observed lower than the seismogenic crustal thickness (e.g., McKenzie, 2015). In this regard, well resolved seismic records across central Australia implicate mostly very shallow depths of <10 km (Attanayake et al., 2020). An exception is the Amadeus Basin where earthquake hypocentres are notably absent in the mid-crust, as

discussed by Jackson and McKenzie (2022), who on that account argue for an effective T_e of about 30 km. We suggest that the geomorphology of the Finke provides a novel constraint on T_e as well as the magnitude and timing of transient variations of in-plane loads acting in continental interiors, as we consider below.

We propose that short-range ($\sim 10^2$ km) flexural responses to large uncompensated loads embedded in the crust and upper mantle (Beekman et al., 1997) led to foretilting that steepened the Finke and drove fluvial incision. And yet, accounting for dynamic switching from incision to aggradation requires a further mechanism that episodically reduces river slopes and sediment transport capacity, thereby promoting accumulation of the thick valley fill. As we have shown, one mechanism for such periodicity is the elastic response to changes in in-plane loading even for moderate load variations of order 1 x 10^{12} N m^{-1}. Modelling studies that explore how shifting plate boundaries influence stress within the Indo-Australian plate generally infer a progressive rise in compressional stress, as seen most dramatically in the mid-late Miocene onset of buckling in the Indian Ocean (e.g., Sandiford et al., 2005). The role of flow beneath the lithosphere has received comparatively less attention. We speculate that variations in long-term loading in this remote, interior part of the plate more likely stem from tractions imposed at the base of the plate rather than plate boundaries, the nearest of which is ~1700 km distant. We consider two mechanisms by which mantle flow may contribute stress transients in the lithosphere. First, given that surface uplift must work against gravity, dynamic topography drives a shift in gravitational potential energy that directly results in a change in stress (Coblentz et al., 1994). Surface uplift of 1 km is equivalent to a gravitational potential energy increase of ~1 x 10^{12} J m^{-2} (equivalent to an in-plane loading of 1 x 10^{12} N m^{-1}) (see Fig. 10). Second, tractions imparted by mantle flow at the base of the lithosphere have long been recognised as a potential contributor to intraplate stress (e.g., Forsyth and Uyeda, 1975), although the magnitude of the contribution is uncertain. In their analysis of the Indo-Australian intraplate stress field, Coblentz et al. (1995) argue that tractions were either negligible or contributed only slightly to resistance to plate motion. However, this assessment is now being challenged. Sandiford et al. (2020) implicate sub-lithospheric processes in subtle deformation observed in major LEB drainage systems running parallel to NNW plate motion. In detail they propose that a pressure-driven mantle flow regime was established with the plate's acceleration at ~43 Ma (mid-Eocene), and that it has contributed to SSW foretilting of order 100 m across the LEB. A distinctive multichannel river pattern, anabranching, is developed extensively along the SSW-flowing Georgina, Diamantina and Cooper systems in the northeast of the LEB. Given that anabranching modulates sediment and water throughput in response to changes in longitudinal slope (Jansen and Nanson, 2004), a compelling explanation for the vast tracts of anabranching in the LEB (and farther east) is the temporal variation in mantle flow resistance around a thickened lithospheric keel that spans much of the continental interior (Sandiford et al., 2020).

In this sense, the LEB may be seen as pivoting on a WNW-ESE axis, tilting southward to a degree that depends on the specific magnitude of the tractions at the base of the lithosphere. We hypothesise that such tractions modulate the long-term flexural response observed at Finke Gorge, which in turn requires the additional precondition of large uncompensated loads. This is a potentially important insight because the amplitude (~100 m) of the flexural response constrains the magnitude of variations in the tractions consistent with changes in T_e of ~10% (~1–2 x 10^{12} N m^{-1}) (e.g., Burov and Diament, 1995). In the face of difficulties with resolving the elastic thickness of the central Australian lithosphere, our hypothesis is consistent with $T_e \sim 30$ km.

Finally, we turn to the question of what limits the flexural response observed in the Finke. As noted by Beekman et al. (1997), the evidence for synchronous long-term uplift and subsidence across the Central Ranges requires some accumulated tectonic strain. We agree and add that the transient elastic response is capable of building and shrinking relief on a similar order. Any accumulation of tectonic strain will be strongly biased to periods of elevated in-plane compression. For most of the Cenozoic there has probably been limited accumulation of active tectonic strain. It is only during transient phases of higher compressional loading ($\Delta\sigma_{xx} \gg 10$ MPa) that appreciable permanent strain accumulates. In restricted locales with low T_e (≤ 35 km) and extreme internal loading, the elastic deformation is enhanced by the compressional loading, as expressed in the upper Finke by tilting and fluvial incision. Conversely, unbuckling accompanies compressional unloading, which back-tilts the upper Finke and promotes aggradation. The cosmogenic nuclide data presented here suggests that the characteristic timescale for these processes is of order 1–10 Ma.

Based on our findings at Finke Gorge, we propose a new perspective on the evolution of the central Australian landscape. Considered in isolation, convective mantle processes modulate surface topography over length-scales of order 10^3 km and are expected to propagate across the LEB in line with plate motion, rather than remain localised to a specific region at its perimeter. We see no direct connection between the geomorphic record in the Finke and the dynamic topography suggested by Schellart and Spakman (2015). Instead, we advocate a subtle relationship between mantle flow and surface topography mediated by the elastic response of the lithosphere to tractions at the base of the plate.

6. Conclusion

Intertwined bedrock valleys are extremely rare in nonglacial, intraplate settings, and the example in the upper Finke has provided a long-lasting enigma. We propose that the remarkable magnitude of incision and aggradation observed in the Finke is rooted in the geodynamic setting of a Palaeozoic intraplate orogen and the rapid northward migration of the Indo-Australian plate. By combining a MCMC inversion model with cosmogenic ^{10}Be and ^{26}Al measurements on palaeovalley gravels at Finke Gorge, we show that the burial-exhumation in the palaeovalley and associated epigenetic gorge incision occurred over a multi-million-year timescale and likely predates the Quaternary. The nuclide memory in the palaeovalley gravels is decoupled from their source ~50 km upstream. Post-Miocene aridification appears to have played a secondary role in these events. We suggest that the fluctuating incision-aggradation phases that led to gorge overprinting reflect flexural responses to transient tectonic loading in the presence of extreme uncompensated loads embedded in the crust. The amplitude of topographic response provides a new insight to the nature of the effective elastic thickness of the central Australian lithosphere. We propose a thickness of ~30 km that varies by ~10% with tectonic loading of ~1–2 x 10^{12} N m^{-1}.

CRediT authorship contribution statement

J.D. Jansen: conceptualization, fieldwork, data analysis, writing. **M. Sandiford:** conceptualization, geodynamic modelling, data analysis, writing. **T. Fujioka:** conceptualization, fieldwork, cosmogenic nuclide sample preparation and measurement, data analysis, writing. **T.J. Cohen:** fieldwork, writing. **M. Struck:** fieldwork, cosmogenic nuclide sample preparation and measurement, data analysis. **S.P. Anderson:** fieldwork, writing. **R.S. Anderson:** conceptualization, fieldwork, data analysis, writing. **K. Wilcken:** accelerator mass spectrometer measurements. **D.L. Egholm:** conceptualization, cosmogenic nuclide inversion modelling, data analysis, writing.

Declaration of competing interest

The authors declare that they have no known competing financial interests or personal relationships that could have appeared to influence the work reported in this paper.

Acknowledgements

We thank A.T. Codilean, G. Ruetenik, P. English, and the late J. Chappell for their insightful discussion, and G. Pickup for supplying the TOPSAR digital elevation data. We thank K. Czarnota and an anonymous reviewer for their constructive recommendations. The research visit of R.S. Anderson and S.P. Anderson in 2015 was funded by an International Partnership Grant from the University of Wollongong. We sincerely acknowledge the Traditional Owners of this Country.

Appendix A. Supplementary material

Supplementary material related to this article can be found online at https://doi.org/10.1016/j.epsl.2022.117456.

References

Alley, N.F., 1998. Cainozoic stratigraphy, palaeoenvironments and geological evolution of the Lake Eyre Basin. Palaeogeogr. Palaeoclimatol. Palaeoecol. 144, 239–263.

Attanayake, J., King, T., Quigley, M.C., Gibson, G., Clark, D., Jones, A., Sandiford, M., 2020. Rupture characteristics and the structural control of the 2016 M_w 6.1 intraplate earthquake in the Petermann Ranges, Australia. Bull. Seismol. Soc. Am. 110, 1037–1045. https://doi.org/10.1785/0120190266.

Baker, V.R., 2021. Landscape evolution in the Finke (Larapinta) River transverse drainage, central mountain ranges, Australia. Stud. Geomorphol. Carpatho-Balcan. 53–54.

Barnett-Moore, N., et al., 2014. Cenozoic uplift of south Western Australia as constrained by river profiles. Tectonophysics 622, 186–197. https://doi.org/10.1016/j.tecto.2014.03.010.

Beekman, F., Stephenson, R.A., Korsch, R.J., 1997. Mechanical stability of the Redbank Thrust Zone, Central Australia: Dynamic and rheological implications. Aust. J. Earth Sci. 44, 215–226. https://doi.org/10.1080/08120099708728305.

Belton, D.X., Brown, R.W., Kohn, B.P., Fink, D., Farley, K.A., 2004. Quantitative resolution of the debate over antiquity of the central Australian landscape: implications for the tectonics and geomorphic stability of cratonic interiors. Earth Planet. Sci. Lett. 219, 21–34.

Bowler, J.M., 1976. Aridity in Australia: age, origins and expression in aeolian landforms and sediments. Earth-Sci. Rev. 12, 279–310.

Braun, J., Robert, X., Simon-Labric, T., 2013. Eroding dynamic topography. Geophys. Res. Lett. 40, 1494–1499. https://doi.org/10.1002/grl.50310.

Burov, E.B., Diament, M., 1995. The effective elastic thickness (T_e) of continental lithosphere: what does it really mean. J. Geophys. Res., Solid Earth 100, 3905–3927.

Célérier, J., et al., 2005. Modes of active intraplate deformation, Flinders Ranges, Australia. Tectonics 24, TC6006. https://doi.org/10.1029/2004tc001679.

Chen, X.Y., Bowler, J.M., Magee, J.W., 1993. Late Cenozoic stratigraphy and hydrologic history of Lake Amadeus, a central Australian playa. Aust. J. Earth Sci. 40, 1–14. https://doi.org/10.1080/08120099308728059.

Child, D., Elliott, G., Mifsud, C., Smith, A.M., Fink, D., 2000. Sample processing for earth science studies at ANTARES. Nucl. Instrum. Methods Phys. Res. B 172, 856–860.

Chmeleff, J., von Blanckenburg, F., Kossert, K., Jakob, D., 2010. Determination of the ^{10}Be half-life by multicollector ICP-MS and liquid scintillation counting. Nucl. Instrum. Methods Phys. Res. B 268, 192–199.

Coblentz, D.D., et al., 1995. The origins of the intraplate stress field in continental Australia. Earth Planet. Sci. Lett. 133, 299–309. https://doi.org/10.1016/0012-821x(95)00084-p.

Coblentz, D.D., Richardson, R.M., Sandiford, M., 1994. On the gravitational potential of the Earth's lithosphere. Tectonics 13, 929–945. https://doi.org/10.1029/94tc01033.

Crossman, S., Li, O., 2015. Surface hydrology lines (national). Geoscience Australia, Canberra. http://pid.geoscience.gov.au/dataset/ga/83130.

Czarnota, K., et al., 2013. Spatial and temporal patterns of Cenozoic dynamic topography around Australia. Geochem. Geophys. Geosyst. 14, 634–658. https://doi.org/10.1029/2012gc004392.

Czarnota, K., et al., 2014. Spatial and temporal patterns of Australian dynamic topography from river profile modeling. J. Geophys. Res., Solid Earth 119, 1384–1424. https://doi.org/10.1002/2013jb010436.

English, P., et al., 2001. Lake Lewis basin, central Australia: environmental evolution and OSL chronology. Quat. Int. 83–85, 81–101. https://doi.org/10.1016/s1040-6182(01)00032-5.

Farr, T.G., et al., 2007. The Shuttle Radar Topography Mission. Rev. Geophys. 45, RG2004. https://doi.org/10.1029/2005RG000183.

Forsyth, D., Uyeda, S., 1975. On the relative importance of the driving forces of plate motion. Geophys. J. Int. 43, 163–200. https://doi.org/10.1111/j.1365-246x.1975.tb00631.x.

Fujioka, T., et al., 2005. Global cooling initiated stony deserts in central Australia 2–4 Ma, dated by cosmogenic ^{21}Ne-^{10}Be. Geology 33, 993–996. https://doi.org/10.1130/g21746.1.

Gurnis, M., 1998. Cretaceous vertical motion of Australia and the Australian Antarctic discordance. Science 279 (5356), 1499–1504. https://doi.org/10.1126/science.279.5356.1499.

Haines, P.W., Hand, M., Sandiford, M., 2001. Palaeozoic synorogenic sedimentation in central and northern Australia: A review of distribution and timing with implications for the evolution of intracontinental orogens. Aust. J. Earth Sci. 48, 911–928. https://doi.org/10.1046/j.1440-0952.2001.00909.x.

Heimsath, A.M., Chappell, J., Fifield, K., 2010. Eroding Australia: rates and processes from Bega Valley to Arnhem Land. Geol. Soc. (Lond.) Spec. Publ. 346 (1), 225–241. https://doi.org/10.1144/sp346.12.

Hindle, D., 2021. flexure-1d-hs. Zenodo. https://doi.org/10.5281/zenodo.4642172.

Hillis, R.R., et al., 1997. Modelling the contemporary stress field and its implications for hydrocarbon exploration. Explor. Geophys. 28, 88–93. https://doi.org/10.1071/eg997088.

Jackson, J., McKenzie, D., 2022. The exfoliation of cratonic Australia in earthquakes. Earth Planet. Sci. Lett. 578, 117305. https://doi.org/10.1016/j.epsl.2021.117305.

Jansen, J.D., Nanson, G.C., 2004. Anabranching and maximum flow efficiency in Magela Creek, northern Australia. Water Resour. Res. 40, W04503.

Jansen, J.D., et al., 2013. Lowland river responses to intraplate tectonism and climate forcing quantified with luminescence and cosmogenic ^{10}Be. Earth Planet. Sci. Lett. 366, 49–58. https://doi.org/10.1016/j.epsl.2013.02.007.

Kirby, J.F., 2014. Estimation of the effective elastic thickness of the lithosphere using inverse spectral methods: the state of the art. Tectonophysics 631, 87–116. https://doi.org/10.1016/j.tecto.2014.04.021.

Knudsen, M.F., Egholm, D.L., 2018. Constraining Quaternary ice covers and erosion rates using cosmogenic. ^{26}Al/^{10}Be nuclide concentrations. Quat. Sci. Rev. 181, 65–75.

Knudsen, M.F., Egholm, D.L., Jacobsen, B.H., Larsen, N.K., Jansen, J.D., Andersen, J.L., Linge, H.C., 2015. A multi-nuclide approach to constrain landscape evolution and past erosion rates in previously glaciated terrains. Quat. Geochronol. 30, 100–113.

Kohl, C., Nishiizumi, K., 1992. Chemical isolation of quartz for measurement of in-situ-produced cosmogenic nuclides. Geochim. Cosmochim. Acta 56, 3583–3587. https://doi.org/10.1016/0016-7037(92)90401-4.

Korschinek, G., et al., 2010. A new value for the half-life of ^{10}Be by heavy ion elastic recoil detection and liquid scintillation counting. Nucl. Instrum. Methods Phys. Res. B 268, 187–191.

Lal, D., 1991. Cosmic ray labeling of erosion surfaces: in situ nuclide production rates and erosion models. Earth Planet. Sci. Lett. 104, 424–439.

Lambeck, K., 1983. Structure and evolution of the intracratonic basins of central Australia. Geophys. J. Int. 74, 843–886. https://doi.org/10.1111/j.1365-246X.1983.tb01907.x.

Lambeck, K., 1984. Structure and evolution of the Amadeus, Officer and Ngalia basins of central Australia. Aust. J. Earth Sci. 31, 25–48. https://doi.org/10.1080/08120098408729278.

Lane, R.J.L., Wynne, P.E., Poudjom Djomani, Y.H., Stratford, W.R., Barretto, J.A., Caratori Tontini, F., 2020. 2019 Australian national gravity grids explanatory notes. Record 2020/22. Geoscience Australia, Canberra.

Lloyd, J.W., Jacobson, G., 1987. The hydrogeology of the Amadeus Basin, central Australia. J. Hydrol. 93, 1–24.

Lubiniecki, D.C., et al., 2020. Cenozoic structural evolution of the Mount Lofty Ranges and Flinders Ranges, South Australia, constrained by analysis of deformation bands. Aust. J. Earth Sci., 1–19. https://doi.org/10.1080/08120099.2019.1695227.

Mabbutt, J.A., 1966. Landforms of the Western Macdonnell Ranges. In: Dury, G.H. (Ed.), Essays in Geomorphology. Heinemann, London, pp. 83–119.

Madigan, C.T., 1931. The physiography of the Western Macdonnell Ranges, central Australia. Geogr. J. 78, 417–433.

McKenzie, D., 2015. A note on estimating T_e from Bouguer coherence. GEM Int. J. Geomath. 7, 103–116. https://doi.org/10.1007/s13137-015-0078-4.

McNutt, M.K., Menard, H.W., 1982. Constraints on yield strength in the oceanic lithosphere derived from observations of flexure. Geophys. J. Int. 71, 363–394.

Mifsud, C., Fujioka, T., Fink, D., 2013. Extraction and purification of quartz in rock using hot phosphoric acid for in situ cosmogenic exposure dating. Nucl. Instrum. Methods Phys. Res. B 294, 203–207. https://doi.org/10.1016/j.nimb.2012.08.037.

Müller, R.D., Sdrolias, M., Gaina, C., Roest, R.W., 2008. Age, spreading rates, and spreading asymmetry of the world's ocean crust. Geochem. Geophys. Geosyst. 9, Q04006. https://doi.org/10.1029/2007GC001743.

Nishiizumi, K., 2004. Preparation of ^{26}Al AMS standards. Nucl. Instrum. Methods Phys. Res. B 223–224, 388–392.

Nishiizumi, K., et al., 2007. Absolute calibration of ^{10}Be AMS standards. Nucl. Instrum. Methods Phys. Res. B 258, 403–413. https://doi.org/10.1016/j.nimb.2007.01.297.

Pickup, G., Allan, G., Baker, V.R., 1988. History, palaeochannels and palaeofloods of the Finke River, central Australia. In: Warner, R.F. (Ed.), Fluvial Geomorphology of Australia. Academic Press, Sydney, pp. 177–200.

Raymond, O., Liu, S., Gallagher, R., Zhang, W., Highet, L., 2012. Surface geology of Australia 1:1 million scale (2012 edn.). Commonwealth of Australia (Geoscience Australia). https://data.gov.au/dataset/surface-geology-of-australia-data-package-2012-edition.

Sandiford, M., 2007. The tilting continent: a new constraint on the dynamic topographic field from Australia. Earth Planet. Sci. Lett. 261, 152–163. https://doi.org/10.1016/j.epsl.2007.06.023.

Sandiford, M., Lawrie, K., Brodie, R.S., 2020. Hydrogeological implications of active tectonics in the Great Artesian Basin, Australia. Hydrogeol. J. 28, 57–73. https://doi.org/10.1007/s10040-019-02046-4.

Sandiford, M., Quigley, M., 2009. TOPO-OZ: insights into the various modes of intraplate deformation in the Australian continent. Tectonophysics 474, 405–416. https://doi.org/10.1016/j.tecto.2009.01.028.

Sandiford, M., Wallace, M., Coblentz, D., 2004. Origin of the in situ stress field in south-eastern Australia. Basin Res. 16, 325–338. https://doi.org/10.1111/j.1365-2117.2004.00235.x.

Sandiford, M., Coblentz, D., Schellart, W.P., 2005. Evaluating slab-plate coupling in the Indo-Australian plate. Geology 33, 113–116.

Schellart, W.P., Spakman, W., 2015. Australian plate motion and topography linked to fossil New Guinea slab below Lake Eyre. Earth Planet. Sci. Lett. 421, 107–116. https://doi.org/10.1016/j.epsl.2015.03.036.

Stone, J., 2000. Air pressure and cosmogenic isotope production. J. Geophys. Res. 105, 23753–23760.

Struck, M., Jansen, J.D., Fujioka, T., Codilean, A.T., Fink, D., Egholm, D.L., Fülöp, R.-H., Wilcken, K.M., Price, D.M., Kotevski, S., 2018a. Soil production and transport on postorogenic desert hillslopes quantified with ^{10}Be and ^{26}Al. Geol. Soc. Am. Bull. 130, 1017–1040.

Struck, M., Jansen, J.D., Fujioka, T., Codilean, A.T., Fink, D., Fülöp, R.-H., Wilcken, K.M., Price, D.M., Kotevski, S., Fifield, K., Chappell, J., 2018b. Tracking the ^{10}Be-^{26}Al source-area signal in sediment-routing systems of arid central Australia. Earth Surf. Dyn. 6, 329–349.

Teyssier, C., 1985. A crustal thrust system in an intracratonic tectonic environment. J. Struct. Geol. 7, 689–700.

Wells, R.T., Callen, R.A. (Eds.), 1986. The Lake Eyre Basin—Cainozoic Sediments, Fossil Vertebrates and Plants, Landforms, Silcretes and Climatic Implications. Australasian Sedimentologists Group Field Guide Series, vol. 4. Geological Society of Australia, Sydney.

Wilcken, K.M., Fujioka, T., Fink, D., Fülöp, R.-H., Codilean, A.T., Simon, K., Mifsud, C., Kotevski, S., 2019. SIRIUS performance: ^{10}Be, ^{26}Al and ^{36}Cl measurements at ANSTO. Nucl. Instrum. Methods Phys. Res. B 455, 300–304.